minerals

MDPI

Article

Ferric Sulfate Leaching of Pyrrhotite Tailings between 30 to 55 °C

Nazanin Samadifard, Cheryl E. Devine, Elizabeth Edwards, Krishna Mahadevan and Vladimiros G. Papangelakis *

Received: 8 October 2015; Accepted: 11 November 2015; Published: 27 November 2015
Academic Editor: William Skinner

Department of Chemical Engineering and Applied Chemistry, University of Toronto, 200 College Street, Toronto, ON M5S-3E5, Canada; nazanin.samadifard@mail.utoronto.ca (N.S.); cheryl.washer@mail.utoronto.ca (C.E.D.); elizabeth.edwards@utoronto.ca (E.E.); krishna.mahadevan@utoronto.ca (K.M.)

* Correspondence: vladimiros.papangelakis@utoronto.ca; Tel.: +1-416-978-1093; Fax: +1-416-978-8605

Abstract: Mine tailings present major environmental issues in the mining industry. However due to the depletion of high-grade sulfide ores for metal recovery, tailings could also be a potential resource for certain valuable metals. The present study investigates the potential to recover nickel from pyrrhotite tailings. Leaching tests were performed in acidic ferric sulfate media with 0.14 wt % solids to keep the ferric concentration essentially constant. The temperature was varied between 30 and 55 °C, and the ferric concentration was in a range 0.02–0.3 M. The results showed that both temperature and ferric sulfate concentration had significant effects on the nickel extraction kinetics. The shrinking core model (SCM) was applied to the nickel extraction data. The rate controlling step was found to be product layer diffusion. The Arrhenius plot yielded an activation energy of Ea = 62.12 kJ/mol based on apparent reaction rates obtained by the SCM. The reaction order with respect to ferric ion was found to be 1 at the high concentration range. SEM images of partially leached tailings confirmed the presence of elemental sulfur around the pyrrhotite particles, which was responsible for the observed non-linear leaching kinetics (diffusion control).

Keywords: nickeliferous pyrrhotite; ferric sulfate leaching; elemental sulfur; shrinking core model

1. Introduction

Due to continuous exploitation, high-grade sulfide ores are gradually being exhausted. Low-grade sulfide minerals, including mining wastes, are being considered as alternative metal resources for the future. Over the past 50 years, the Sudbury region in Ontario, Canada, has accumulated 50–100 million tonnes of pyrrhotite tailings as a consequence of the local smelting operations [1]. These tailings could be a significant low-grade nickel resource, if a low-cost process for nickel recovery could be developed. In addition, environmental hazards like acid mine drainage (AMD) could be reduced by treating the pyrrhotite tailings. Previously, several pyrometallurgical processes were investigated for the treatment of the pyrrhotite tailings [1–4]; however, most were abandoned due to the production of SO_2 gas during the roasting process and the introduction of additional Fe in the slag. Although hydrometallurgical processes for nickel recovery would offer the advantage of eliminating SO_2 emissions, limited laboratory studies have been performed using techniques such as acid leaching by hydrochloric and nitric acid, or by high-pressure oxidation [5–7]. Recently, a bioleaching process was also investigated as an alternative hydrometallurgical process in our laboratory [8]. In this process concept, pyrrhotite and pentlandite, the two principal nickel carriers in the tailings are leached by ferric sulfate, which is regenerated with microbial assistance.

Ferric ion is a strong oxidizing agent that plays an important role in oxidation of sulfide ores. A few studies have been conducted on the leaching of pyrrhotite in ferric sulfate solution [9–11], although the direct effect of ferric ion on the oxidation of pyrrhotite tailings has not been systematically studied. Earlier studies have shown that elemental sulfur is the dominant product of the ferric sulfate leaching of pyrrhotite [12,13]. This is advantageous over the production of sulfuric acid as a by-product, which would require recovery, storage, or neutralization, and impoundment of vast amounts of gypsum, which would make the process uneconomical.

The aim of this work was to study the leaching kinetics of nickeliferous pyrrhotite tailings in concentrated ferric sulfate media under abiotic conditions and develop a kinetic model that can be used for process design. The results of this study would be very useful in any follow-up bioleaching study, as it would set a baseline for the chemical performance of the system.

2. Materials and Methods

2.1. Characterization of Tailings

Upgraded pyrrhotite tailings were obtained from Vale's nickel milling operations in Sudbury, ON, Canada. The slurry was delivered in a 20 kg container containing deoxygenated water due to the reducing and reactive nature of pyrrhotite. A core sample was taken, homogenized using a heavy-duty impeller, and subsequently vacuum-filtered through Whatman quantitative filter paper and collected as several small cakes. The cakes were stored in double-sealed plastic bags at −20 °C to minimize surface oxidation by oxygen in air. One day prior to any experiment, samples were thawed at 4 °C, and the moisture content was determined by weighing, vacuum drying, and reweighing a subsample at the time of experimental setup. This subsample was later digested in aqua regia (1:3 HNO_3:HCl), diluted in 5% HNO_3 and subjected to elemental analysis via inductively coupled plasma-optical emission spectrometry (ICP-OES), Agilent Technologies 700 series. Although the exact composition of the pyrrhotite tailings produced at the Sudbury facility may vary with the ore being processed, the average composition of at least 50 samples studied is shown in Table 1. The most abundant elements in the pyrrhotite tailings are Fe (52.81 ± 2.50 wt %), S (32.00 ± 1.29 wt %), and Ni (1.00 ± 0.02 wt %). Mineralogical characterization of the tailings sample was determined by QEMSCAN (FEI, Hilsboro, OR, USA) at SGS Lakefield, ON, Canada, and is summarized in Table 2. Monoclinic pyrrhotite (Fe_7S_8) is dominant at 86.2 wt %, whereas pentlandite ($(Fe,Ni)_9S_8$) accounts for only 1.2 wt % of the tailings although it holds 40% of the total nickel. The balance of 60% is associated with pyrrhotite.

In all cases, the particle size distribution (PSD) of the pyrrhotite tailings was measured using a Malvern Mastersizer 2000 (Malvern Instruments, Malvern, UK). A typical distribution in Figure 1 shows the presence of fine particles at about 20 vol % below 10 μm. The average particle size in most experiments was 32 μm with a d50 of 28 μm and a coefficient of variation (CV) of 0.82.

Table 1. Elemental composition of pyrrhotite tailings.

Element	Concentration (wt %)
Fe	52.81 ± 2.5
S	32.00 ± 1.29
Ni	1.00 ± 0.02
Al	0.38
Cu	0.28
Ca	0.28
Mg	0.18
Co	0.02
Mn	0.02
Cr	0.01

Table 2. Mineralogical composition of pyrrhotite tailings.

Mineral	Chemical Formula	wt %
Pyrrhotite	Fe_7S_8	86.2
Pentlandite	$(Fe,Ni)_9S_8$	1.2
Chalcopyrite	$CuFeS_2$	0.7
Pyrite	FeS_2	0.4
Silicates	Mg_2SiO_4	3.8
Fe-(Ti) Oxides	Fe_3O_4, $FeTiO_3$	4.6
Quartz	SiO_2	3.1

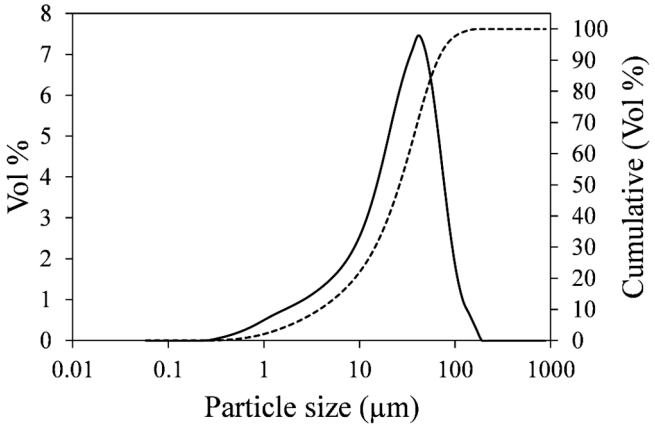

Figure 1. Particle size distribution (solid line) and cumulative curve (dotted line) of pyrrhotite tailings.

2.2. Leaching Tests

Leaching experiments were conducted in 500 mL baffle-based Erlenmeyer flasks, and were designed to test sulfide mineral leaching rates, extents and products at different temperatures and ferric ion concentrations, as summarized in Table 3. In all case, flasks were filled with 500 mL of a solution containing 0.2 N H_2SO_4 and a known concentration of ferric sulfate, and then heated to the desired temperature (30, 40, or 55 °C). Ferric sulfate concentrations selected (0.02–0.3 M) corresponded to 1.1–17.6 excess stoichiometric levels with respect to monoclinic pyrrhotite based on the following overall reaction:

$$Fe_7S_8 + 7Fe_2(SO_4)_3 \rightarrow 21FeSO_4 + 8S^0 \quad (1)$$

Table 3. Experimental matrix for the leaching tests.

Experiment	Ferric Sulfate Concentration (M)	Stoichiometric Excess Reaction (1)	Temperature (°C)	Elemental S Analysis
A1	0.12	7.5	30	-
A2	0.12	7.5	40	-
A3	0.12	7.5	55	-
B1	0.02	1.2	55	-
B2	0.1	6.6	55	-
B3	0.2	12	55	-
B4	0.3	17.6	55	-
C1	0.2	12	40	HPLC
C2	0.2	12	55	HPLC
D1	0.2	3	55	SEM

The reaction was initiated by adding about 0.7 g (0.14 wt %) of the upgraded pyrrhotite tailings to the solution, except in Experiment D1, which was designed to observe the morphology of elemental

sulfur on partially leached pyrrhotite particles. In this case, 2.8 g of tailings was added into 500 mL leach solution containing 0.2 M ferric sulfate and 0.2 M sulfuric acid at 55 °C. The flasks were then capped with aluminum foil to prevent cross-contamination, and placed in an orbital shaker set to the desired temperature and 250 rpm, a rate that had been visually determined to be sufficient to achieve complete solid suspension. At regular time intervals the shaker was stopped and the flasks were weighed to determine the mass of water that had evaporated. The evaporated water loss was made up by adding an equal volume of deionized water. The flasks were mixed thoroughly by shaking to keep the pulp density uniform, and 5 mL of slurry samples were removed and immediately filtered using 0.45 μm syringe filters. The filtrate was analyzed for oxidation reduction potential (ORP), pH, nickel and ferrous ion concentration. Experiments A1-A3 and B1-B4 were performed in triplicate, while in the case of Experiment C1-C2 and D1, four to six separate flasks were prepared and at each timepoint the contents of one flask were filtered and analyzed for elemental sulfur along with aqueous phase measurements taken in all remaining flasks. Control experiments containing no pyrrhotite tailings were also performed to ensure negligible (<1%) ferrous ion oxidation over the course of the experiments.

To extract elemental sulfur from the leach slurry in Experiments C1-C2, a combination of the techniques described by Dutrizac [14], and McGuire and Hamers [15] was used. At the end of the leaching test the contents of the flask were vacuum filtered with a 10 cm Buchner filter using 15 cm Whatman filter paper. To remove any sulfur from the walls, the flask was rinsed several times with water followed by filtration. The residue was then washed twice with a weak sulfuric acid solution (pH = 3) to remove metal ions and most sulfate ions entrained in the pores of the residue. The filter paper with the leach residue was dried in a vacuum oven at 40 °C overnight. To extract elemental sulfur from the residue, the filter paper was folded several times and placed for 24 h in a beaker containing 50 mL of perchloroethylene (PCE), min. purity 99%. After sulfur extraction, the PCE solution was filtered using a 0.2 μm nylon syringe filter, then diluted 50–200x with PCE to bring the concentration of the sample to within the linear range of standard solutions. Standard solutions for elemental sulfur analysis were prepared within the range of 6–240 mg/L using a procedure similar to that employed by McGuire and Hamers [15]. The samples and the standards were then analyzed for elemental sulfur using High Performance Liquid Chromatography (HPLC). To measure any elemental sulfur that might exist on the pyrrhotite surface prior to leaching, a known amount of the initial sample (~0.25 g) was submerged in 25 mL PCE for 24 h and subjected to the same HPLC analysis.

2.3. Analytical Methods

Liquid samples obtained during the leaching experiments were analyzed for total dissolved iron, nickel and other metals using ICP-OES. The ferrous ion concentration in liquid samples was determined via potentiometric titration with a 0.01 M potassium dichromate solution, according to standard methods [16]. The titration was performed using a Titroline 5000 (SI Analytics USA, College Station, TX, USA), and a graph of mV *vs.* volume of titrant was used to determine the point of inflection. The concentration of elemental sulfur was measured using HPLC with a Dionex 3000 HPLC system (Thermo Scientific, Bannockburn, IL, USA) having a 20 μL injection volume and a Dionex UV detector operating at 254 nm with a 5 nm bandwidth. A Dionex Acclaim 120 C18 reverse-phase column (4.6 × 250 mm; 5 μm) was used with a mobile phase composed of 95% methanol (HPLC Grade, min. purity 99.9%) and 5% water (0.2 μm filtered) at a flow rate of 1 mL/min. The eluent was degassed prior to use with helium. Each measurement lasted for 25 min, and the peak corresponding to the elemental sulfur appeared between 15 and 20 min, due to small changes in the eluent composition.

In Experiment D1, the presence of elemental sulfur on unreacted and reacted pyrrhotite tailings was visualized on polished epoxy mounts using a JEOL JSM-840 Scanning Electron Microscope (SEM) (JEOL, Tokyo, Japan), utilizing back-scattered electrons (BSE) at 15 keV accelerating potential

difference. Energy-dispersive X-ray (EDX) spectra was obtained with the same instrument. About 1 g of the solid sample was gently dispersed in epoxy and adequate time was allowed to ensure that the material was fully cured (about 24 h). The sample mount was gently ground and polished with a 1200 grit silicon carbide paper under running water and then subjected to SEM analysis.

3. Results and Discussion

3.1. Effect of Temperature on Nickel Extraction

The effect of temperature on the kinetics of nickel extraction from the upgraded pyrrhotite tailings is shown in Figure 2. These results were obtained by leaching about 0.14 wt % solids in acidic ferric sulfate solution at 30, 40, and 55 °C, 0.12 M $Fe_2(SO_4)_3$, and 0.2 M H_2SO_4 (Experiments A1-A3). A low % solids value was used to ensure near constant ferric concentration in order to apply the Shrinking Core Model. About 90% of the nickel in the tailings sample was extracted within 50 h at 55 °C, whereas at 30 and 40 °C the observed nickel extraction rate at any given time was lower. In all cases the total nickel in solution appeared to level off before complete dissolution (Figure 2, dotted lines), with higher temperatures corresponding to higher total nickel extraction. Curve fittings in Figure 2 (solid lines) were made with the diffusion-control shrinking core model (SCM) as discussed below.

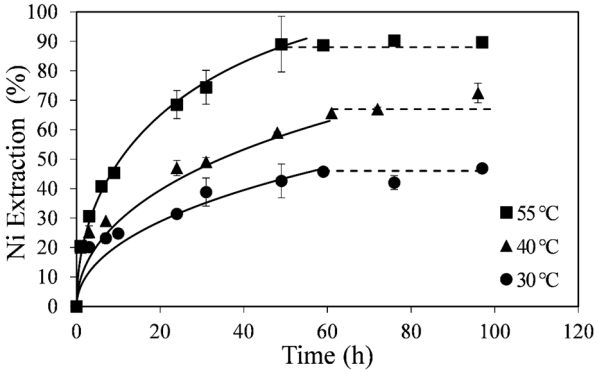

Figure 2. Effect of temperature on nickel extraction kinetics. Conditions: 0.14 wt % solids, 0.12 M $Fe_2(SO_4)_3$ and 0.2 M H_2SO_4. The error bars represent standard deviation of triplicate tests.

The extraction of nickel from the pyrrhotite tailings involves a reaction between $Fe_2(SO_4)_3$ and the nickel-containing sulfide minerals pyrrhotite and pentlandite, which exist as a mixture. Although tailings are non-uniform particulate material in terms of composition and size, the SCM was tested as a semi-empirical kinetics model for the overall nickel dissolution kinetics [17]. The nickel extraction *vs.* time data at different temperatures were plotted for three rate-controlling forms of the SCM: liquid film diffusion (Equation (2)); diffusion through the product layer (Equation (3)); and chemical reaction (Equation (4)), where k_m, k_d and k_r are the apparent reaction rate constants, and x is the fraction of the solid converted.

$$x = k_m t \quad (2)$$

$$1 - 3(1-x)^{2/3} + 2(1-x) = k_d t \quad (3)$$

$$1 - (1-x)^{1/3} = k_r t \quad (4)$$

Since the curves in Figure 2 are not linear, liquid film diffusion (Equation (2)) was ruled out as a controlling process. The straight-line plots in Figure 3 show higher correlation coefficients for all the temperatures in comparison to the chemical reaction-control SCM (Figure 4). Moreover, in Figure 3, the fitted lines at different temperatures extrapolate through the origin or are very close to the origin,

whereas in Figure 4 they do not. Apparent diffusion-control rate constants (k_d), obtained from the slopes of the linear fits in Figure 3, are shown in Table 4.

Table 4. Apparent rate constant values for diffusion control (k_d) at various temperatures.

Temperature (°C)	k_d (h^{-1})
55	1.05×10^{-2}
40	0.32×10^{-2}
30	0.16×10^{-2}

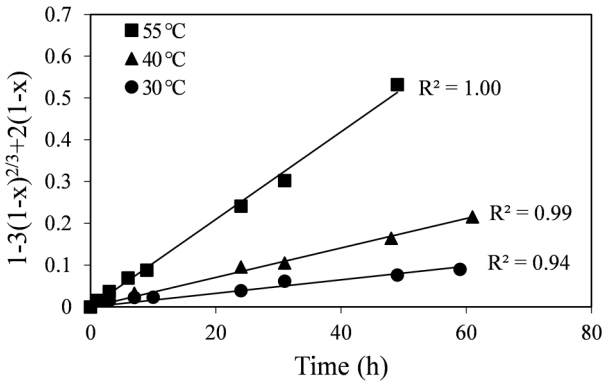

Figure 3. Plot of the diffusion-control SCM *vs.* time at different temperatures.

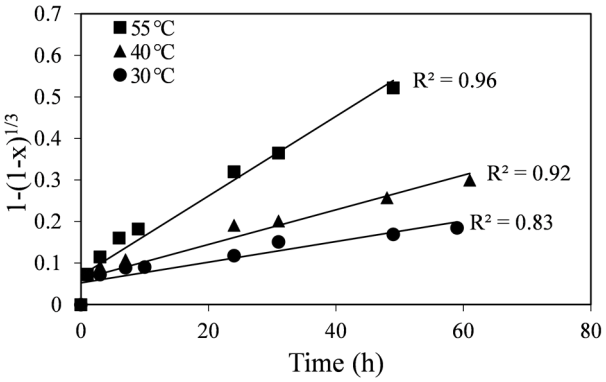

Figure 4. Plot of the chemical reaction-control SCM *vs.* time at different temperatures.

The k_d values obtained were used in an Arrhenius plot shown in Figure 5. The linear fit to the data in Figure 5 gave an activation energy value of E_a = 62.12 kJ/mol with a correlation coefficient close to unity (R^2 = 0.99). This is a high activation energy value commonly attributed to chemical reaction-control processes rather than diffusion-control processes, since the former are more sensitive to temperature than the latter [17]. However, a number of kinetic studies on different systems have reported high values of activation energy for diffusion-control dissolution of sulfide minerals [18,19]. Particle size variability within a sample may affect the interpretation of leaching data when the SCM is applied; for example, Gbor and Jia [20] showed mathematically that when the coefficient of variation (CV) of the PSD is large (0.7 < CV < 1.5), a chemical reaction control process can be mistakenly interpreted as an inert layer diffusion control process. The CV of the PSD of the pyrrhotite tailings was found to be within this range (0.82), however, accounting for the PSD according to Gbor and Jia [20] resulted in a better fit for the diffusion control process (data not shown). The temperature dependent levelling off of nickel concentrations is also more consistent with the formation of a product layer that may limit and ultimately stop the reaction.

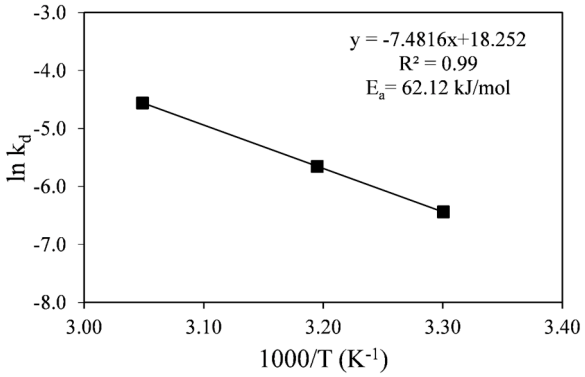

Figure 5. Arrhenius plot for the diffusion-control process.

The fact that the tailings are composed of two individual nickel-bearing minerals, each containing almost half of the total nickel, may complicate things. To obtain an accurate kinetic model for nickel extraction, the oxidation kinetics of pyrrhotite and pentlandite need to be known separately. This information needs to become available by tracking the conversion of each individual mineral in the mixture. A method proposed by Ingraham *et al.* [21], based on the idea that pyrrhotite is an acid soluble mineral, while pentlandite is essentially not acid soluble could be applied to the pyrrhotite tailings. Given the very small amount of pentlandite (1.2 wt %) in the tailings and the experimentation under very low percent solids (~1.4 wt %), it was not possible to achieve this in the present study, and therefore we decided to treat the tailings as a uniform mixture until we develop a mineral separation (physical or chemical) protocol.

3.2. *Effect of Ferric Sulfate Concentration on Nickel Extraction*

The effect of ferric sulfate concentration on the percent extraction of nickel at 55 °C is shown in Figure 6. As expected, the rate of nickel extraction increased with increasing ferric sulfate concentration from 0.02 to 0.3 M. At 0.3 M ferric sulfate, 96% nickel extraction was achieved by about 30 h of retention time. At lower concentrations of ferric sulfate, the kinetics were slower and the extraction curves tended to reach a plateau before complete dissolution of the tailings was achieved. The curve fitting in Figure 6 was made with the diffusion-control SCM. The diffusion-control SCM produced linear fits with higher correlation coefficients for all ferric sulfate concentrations tested than the chemical reaction-control SCM. Apparent diffusion-control rate constants (k_d), shown in Table 5, were obtained from the slopes of the linear fits.

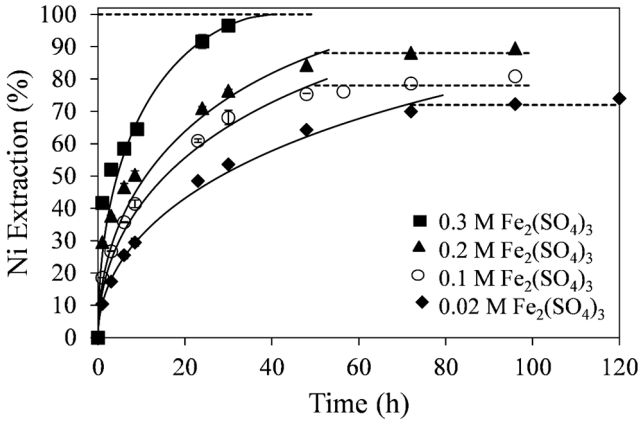

Figure 6. Effect of $Fe_2(SO_4)_3$ concentration on nickel extraction kinetics. Conditions: 55 °C, 0.14 wt % solids, and 0.2 M H_2SO_4. The error bars represent standard deviation from triplicate tests.

Table 5. Diffusion-control apparent rate constants at various concentrations of ferric sulfate.

$Fe_2(SO_4)_3$ (M)	k_d (h^{-1})	R^2
0.3	2.50×10^{-2}	0.99
0.2	1.00×10^{-2}	0.97
0.1	0.71×10^{-2}	0.98
0.02	0.39×10^{-2}	0.99

Using the mixed solvent-electrolyte (MSE) chemical model of the OLI software (OLI Analyzer Studio 3.2; Cedar Knolls, NJ, USA), the concentrations of different Fe species were calculated at 55 °C, 0.2 M H_2SO_4, and different ferric sulfate concentrations (0.02–0.3 M). It can be seen in Table 6 that ferric ion was found to be the dominant species, while $Fe(OH)^{2+}$ concentration was low and did not vary significantly over the range of ferric sulfate concentrations tested. Therefore, the order of reaction was determined with respect to ferric ion concentration.

Table 6. Concentrations of Fe species obtained using OLI-MSE model.

$Fe_2(SO_4)_3$ (M)	Fe^{3+} (M)	$Fe(OH)^{2+}$ (M)
0.3	0.597	0.0031
0.2	0.396	0.0038
0.1	0.196	0.0037
0.02	0.039	0.0011

A plot of the $\log_{10}$ of k_d against the $\log_{10}$ of ferric concentration is shown in Figure 7. The linear fit to the data indicates that the order of reaction with respect to ferric ion is about 0.6. However, the order of reaction with respect to ferric ion within the range of 0.1 to 0.3 M ferric sulfate gives a value of 1.0, which is consistent with the expected value for a diffusion-control process, since Fick's law is first order with respect to diffusing species. This discrepancy is likely due to the fact that at 0.02 M ferric sulfate the stoichiometric ratio of ferric sulfate: pyrrhotite is only 1.2:1 and would therefore not meet the requirements for the use of the SCM, where the concentration of the reactant is required to remain constant during the reaction. Therefore, the lowest ferric sulfate concentration (0.02 M) was ruled out for determination of the reaction order with respect to ferric ion.

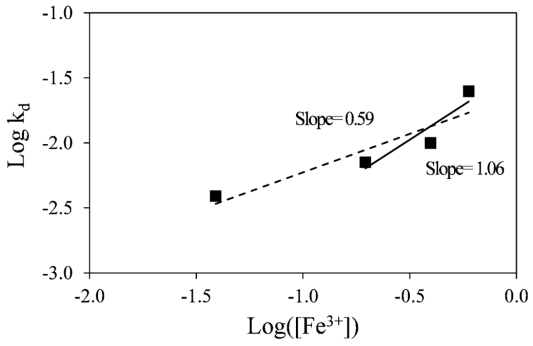

Figure 7. Determination of reaction order with respect to ferric ion.

3.3. Elemental Sulfur Formation

The extraction of nickel and elemental sulfur formation with time at 55 °C, 0.2 M $Fe_2(SO_4)_3$, and 0.2 M H_2SO_4 is shown in Figure 8 (Experiment C1). Each pair of points represents a separate flask, since the low percent solids employed did not permit sufficient slurry sampling for sulfur analysis. As in previous experiments, the pyrrhotite tailings dissolved relatively quickly, and after about 50 h 85% extraction of nickel was achieved. After the same period of time about 75% of the sulfide in

the pyrrhotite tailings had been converted into elemental sulfur. Although the nickel extraction and sulfur production curves follow a similar trend, the elemental sulfur extraction is consistently lower. The difference should be the amount of sulfide oxidized to sulfate ions, although the amount of sulfate could not be determined due to the high sulfate background in the ferric sulfate solution.

The molar ratios of Fe^{2+}/S^0 and Ni^{2+}/S^0 with time are shown in Figure 9. These were calculated from data shown in Figure 8. Initially (at ~1 h), the molar ratios of Fe^{2+}/S^0 and Ni^{2+}/S^0 are high suggesting that the dissolution of the tailings at the beginning of leaching does not produce as much elemental sulfur as at later stages of reaction. This is likely due to the direct acid attack of pyrrhotite with the formation of dissolved hydrogen sulfide, shown in Equation (5). However, as no noticeable gaseous hydrogen sulfide was detected, it is possible that subsequent oxidation of hydrogen sulfide by ferric ions occurs at a slower rate according to Equation (6). In any case, initial surface oxidation of sulfides in the tailings could not account for the initially seen high ratios. These values were determined to be about 1%–2% of total nickel in the tailings samples. The lines in Figure 9 are least-square linear fits to the data points (excluding t = 1 h), producing a Fe^{2+}/S^0 ratio of 2.26 and the Ni^{2+}/S^0 ratio of 0.022.

$$Fe_7S_8 + 14H^+ \rightarrow 7H_2S + 7Fe^{2+} + S^0 \quad (5)$$

$$H_2S + 2Fe^{3+} \rightarrow 3Fe^{2+} + 2H^+ + S^0 \quad (6)$$

$$Fe_7S_8 + 14Fe^{3+} \rightarrow 21Fe^{2+} + 8S^0 \quad (7)$$

It can be seen in Reaction (7) that if monoclinic pyrrhotite were completely dissolved, the molar ratio of Fe^{2+}/S^0 would be 2.6. The fact that the pyrrhotite tailings are not pure and contain small quantities of other sulfide minerals (pentlandite, pyrite and chalcopyrite) may explain the difference between the expected and observed values.

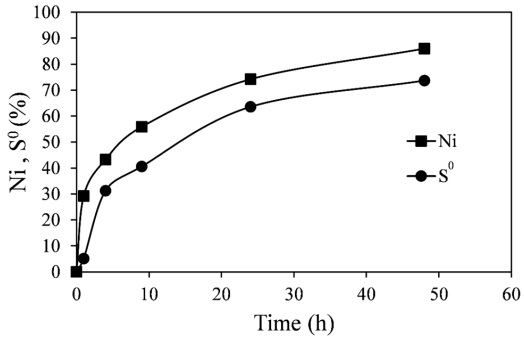

Figure 8. Extraction of Ni and S^0 formation from leaching of pyrrhotite tailings. Conditions: 55 °C, 0.14 wt % solids, 0.2 M $Fe_2(SO_4)_3$, and 0.2 M H_2SO_4.

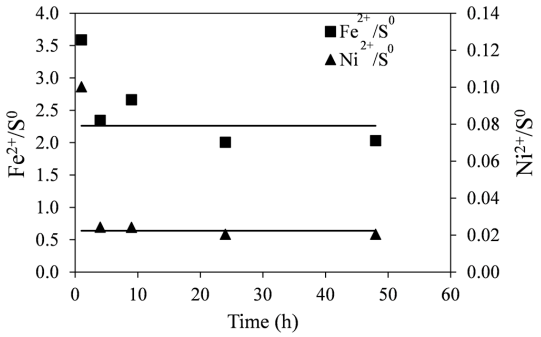

Figure 9. Molar ratios of Fe^{2+}/S^0 and Ni^{2+}/S^0 generated during leaching of pyrrhotite tailings. Conditions: 55 °C, 0.14 wt % solids, 0.2 M $Fe_2(SO_4)_3$, and 0.2 M H_2SO_4. The lines are least square linear fits to the data excluding the first time point (1 h).

Pyrrhotite is the dominant mineral of the tailings (86.2 wt %), and therefore most of the elemental sulfur produced is the by-product of pyrrhotite dissolution. However, nickel in the tailings is attributed to both pentlandite and pyrrhotite, accounting for 40% and 60% of the total nickel, respectively. Accordingly, if pyrrhotite and pentlandite were to react at different rates, the Ni^{2+}/S^0 ratio would be expected to change during the reaction. However, as seen in Figure 9, the Ni^{2+}/S^0 ratio remains relatively constant over time. This suggests that the dissolution rates of pyrrhotite and pentlandite are similar, and that no significant galvanic interaction has occurred between the two minerals, most likely due to their high degree of liberation. This supports the use of the SCM for the analysis of the dissolution kinetics. The theoretical value of Ni^{2+}/S^0 obtained based on the assumption that pyrrhotite and pentlandite react at a similar rate is 0.02 which is comparable with the molar ratios obtained for both 55 and 40 °C (Ni^{2+}/S^0 = 0.022).

To examine whether ferrous ion is re-oxidized to ferric ion due to oxygen entrainment, a control experiment was conducted in which 0.02 M ferrous ion was added to 0.2 M ferric sulfate solution at 55 °C and 250 rpm. After one week, the concentration of ferrous ion remained reasonably constant over time (1% overall reduction). This suggests that there was no oxygen entrainment in these tests, and all oxidative reactions are due to ferric attack.

Figure 10 shows the extraction of nickel and elemental sulfur formation from the leaching of the pyrrhotite tailings at a lower temperature of 40 °C, 0.2 M $Fe_2(SO_4)_3$ and 0.2 M H_2SO_4, where each pair of points represents a separate experiment.

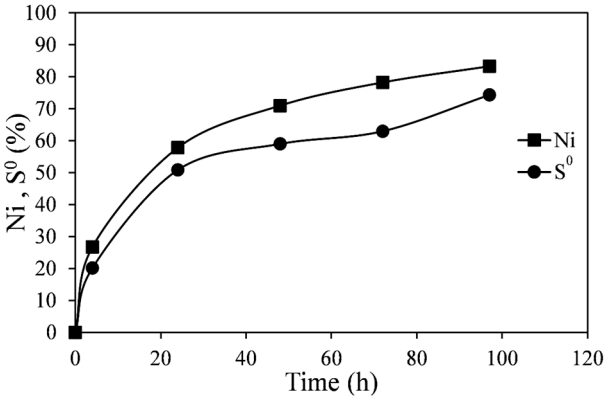

Figure 10. Extraction of Ni and S^0 formation from leaching of pyrrhotite tailings. Conditions: 40 °C, 0.14 wt % solids, 0.2 M $Fe_2(SO_4)_3$, and 0.2 M H_2SO_4.

It can be seen in Figure 10 that after about 100 h, 80% of nickel is extracted, while only about 70% of sulfide is converted to elemental sulfur. Although the curve for elemental sulfur follows a similar trend to that of nickel, the elemental sulfur conversion is consistently lower due to a small fraction (about 20%) converting to sulfate, as explained above.

Figure 11 shows the molar ratios of Fe^{2+}/S^0 and Ni^{2+}/S^0 with time from data in Figure 10. The lines are least-square linear fits to the data points, where the ratios of Ni^{2+}/S^0 and Fe^{2+}/S^0 are 2.62 and 0.022, respectively. The relatively constant Ni^{2+}/S^0 ratio shows that the rates of nickel extraction from both pyrrhotite (60% of total Ni) and pentlandite (40% of total Ni) must be very similar. The constant molar ratios of Ni^{2+}/S^0 and Fe^{2+}/S^0 are similar at both temperatures of 40 and 55 °C indicating that the measured elemental sulfur yield was essentially independent of the temperature of the leach solution. Figure 12 shows that the ORP and pH values of the leach solution remain relatively constant at both temperatures.

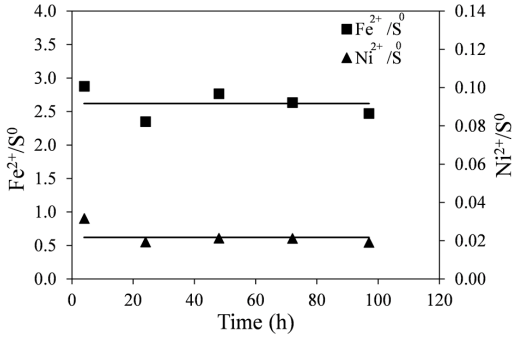

Figure 11. Molar ratios of Fe^{2+}/S^0 and Ni^{2+}/S^0 generated during leaching of pyrrhotite Tailings. Conditions: 40 °C, 0.14 wt % solids, 0.2 M $Fe_2(SO_4)_3$, and 0.2 M H_2SO_4. The lines are least-square linear fits to the data.

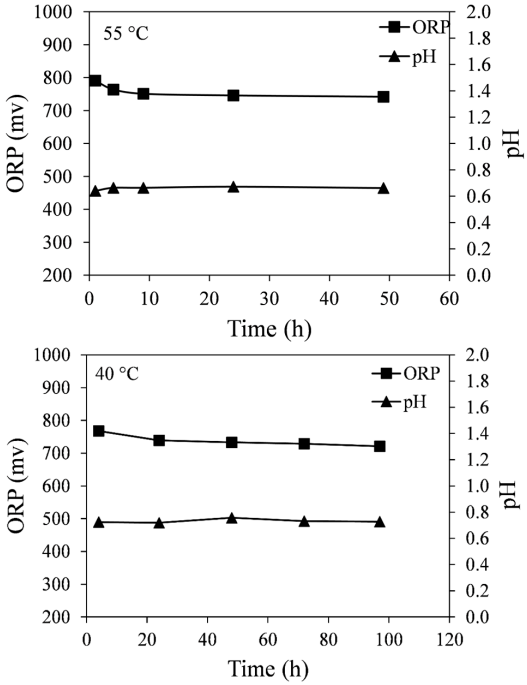

Figure 12. ORP and pH values of the leach solution measured at different times for 55 and 40 °C. Conditions: 0.14 wt % solids, 0.2 M $Fe_2(SO_4)_3$, and 0.2 M H_2SO_4.

3.4. Morphology of Elemental Sulfur

To observe elemental sulfur and its morphology on partially leached pyrrhotite particles at different percent extractions of nickel, Experiment D1 was performed by adding about 2.8 g of the pyrrhotite tailings into 500 mL leach solution containing 0.2 M ferric sulfate and 0.2 M sulfuric acid at 55 °C. After 19, 72, and 144 h of leaching, the contents of the flasks were vacuum filtered, and the residues were dried, epoxy mounted, polished, and subjected to SEM examination. The ICP analysis of the leach solutions showed that the 19, 72, and 144 h of leaching correspond to 50%, 80% and 90% nickel extractions, respectively. These values are lower than those obtained with 1.4 g/L of initial solids loading due to different stoichiometric excess of ferric ion.

The SEM-BSE images of the leached pyrrhotite particles at 0% (a), 50% (b), 80% (c), and 90% (d) nickel extractions are shown in Figure 13. Clearly, a distinct and growing layer of elemental sulfur develops on the pyrrhotite particles. Figure 13b,d shows that a relatively porous sulfur layer forms, which allows the diffusion of the reactants to the reacting interface. This is consistent with the

postulated SCM for diffusion through the product layer-control processes. It seems, however, that as the layer grows it reaches a point that halts the reaction. This phenomenon is less apparent as the temperature increases and accelerates the rate of sulfur formation, perhaps allowing sulfur to remain amorphous and porous for a longer time allowing the completion of iron and nickel dissolution. Elemental mapping of a pyrrhotite particle after 90% nickel extraction was obtained with the help of EDX and is shown in Figure 14.

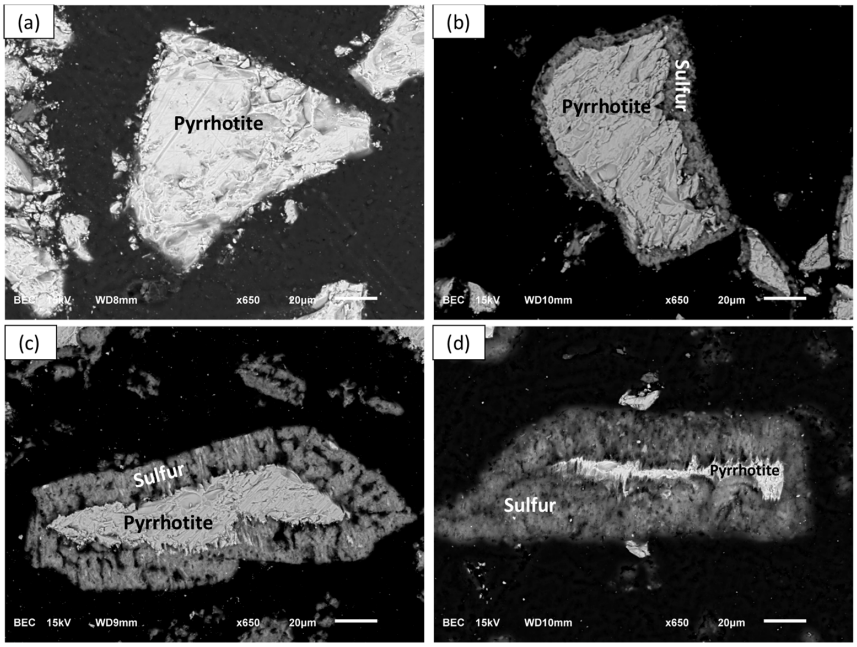

Figure 13. SEM-BSE images of partially leached pyrrhotite particles after (**a**) time 0 (0%); (**b**) 19 h (50%); (**c**) 72 h (80%) and (**d**) 144 h (90%) of leaching. Conditions: 55 °C, 0.56 wt % solids, 0.2 M $Fe_2(SO_4)_3$, and 0.2 M H_2SO_4.

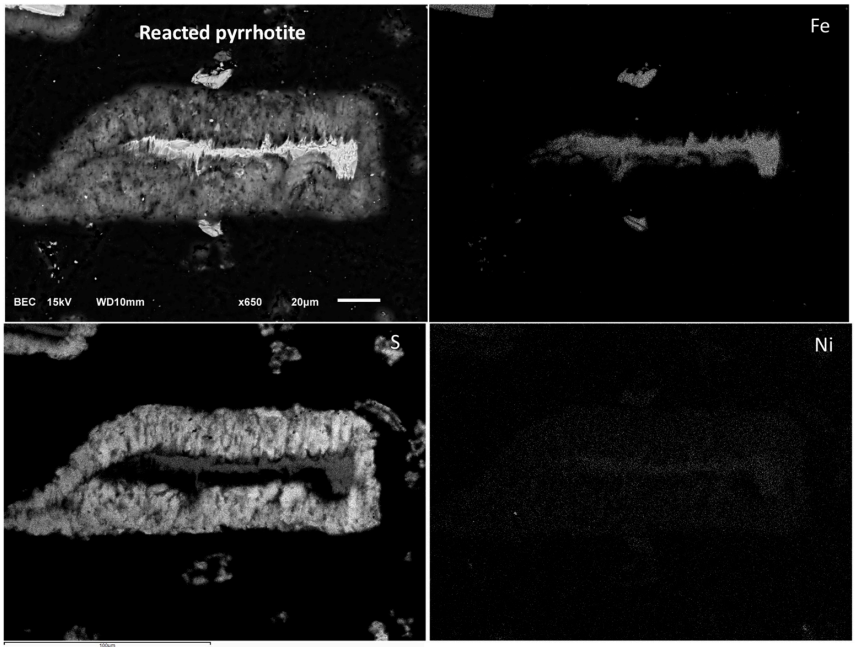

Figure 14. Elemental maps of a pyrrhotite particle after 90% nickel extraction. Conditions: 55 °C, 0.56 wt % solids, 0.2 M $Fe_2(SO_4)_3$, and 0.2 M H_2SO_4.

4. Conclusions

The present work investigated the dissolution kinetics of pyrrhotite tailings from Sudbury, Ontario, Canada, in concentrated ferric sulfate media. The effect of temperature on nickel extraction kinetics was investigated, and the dissolution mechanism of the tailings was determined using the SCM. The diffusion-control kinetic model best fitted the nickel extraction data within the temperature range studied (30–55 °C) with an activation energy value of 62.12 kJ/mol. The reaction order with respect to Fe^{3+} (as opposed to total Fe(III)) was found to be 1 for ferric sulfate concentrations ranging from 0.1 to 0.3 M (6.6 to 17.6x stoichiometric excess).

The results of this study suggest that the overall dissolution process of the pyrrhotite tailings is governed by diffusion through the sulfur product layer. The molar ratios of Fe^{2+}/S^0 and Ni^{2+}/S^0 at 40 °C were about 2.62 and 0.022, respectively, regardless of time. Similar values of the molar ratios were obtained at 55 °C, where Fe^{2+}/S^0 ratio was 2.26 and Ni^{2+}/S^0 ratio was 0.022. The Fe^{2+}/S^0 ratios compare well with the theoretical value of 2.6 based on reaction stoichiometry, whereas the constant Ni^{2+}/S^0 ratio is indicative of a similarity between the dissolution rates of both pyrrhotite and pentlandite.

SEM-BSE images showed a distinct and relatively porous layer of elemental sulfur around the leached pyrrhotite particles. Continuation of the leaching process resulted in a progressive thickening of the sulfur layer to the point of reaction stoppage at certain extraction levels, depending on temperature. This is consistent with the observed non-linear leaching kinetics (diffusion control).

Acknowledgments: Financial support of Vale Canada, Glencore (Sudbury Integrated Nickel Operations), the Ontario Centers of Excellence (OCE), the Centre for Excellence in Mining Innovation (CEMI), and the Natural Sciences and Engineering Research Council of Canada (NSERC) are gratefully acknowledged.

Author Contributions: Nazanin Samadifard, performed all the experimental and analytical work, as well as the processing and interpretation of the results as part of her Masters in Applied Science. Cheryl E. Devine, a Post Doctoral Fellow, assisted in experimental and theoretical matters. Elizabeth Edwards, and Krishna Mahadevan had intellectual input in the areas relating to the bioleaching potential of pyrrhotite tailings. Vladimiros Papangelakis was the Principal Investigator of this work, Thesis supervisor and final paper editor.

Conflicts of Interest: The authors declare no conflict of interest.

References

1. Peek, E.; Barners, A.; Tuzun, A.M. Nickeliferous Pyrrhotite—"Waste or resource?". *Miner. Eng.* **2011**, *24*, 625–637. [CrossRef]
2. Thompson, R.B.; Roesner, G. Fluid bed roasting—Principles and practice. In *Extractive Metallurgy of Copper Nickel and Cobalt*; Queneau, P., Ed.; The Minerals Metals and Materials Society: Warrendale, PA, USA, 1961.
3. Queneau Paul, E.; William Sproul, K.; Illis, A. Method of Producing High-Grade Iron Oxide from Ores Rich in Nickeliferous Pyrrhotite. U.S. Patent 2556215, 12 June 1951.
4. Queneau Paul, E.; William Sproul, K.; Clyde, N.J.G. Method for Producing High Grade Hematite from Nickeliferous Iron Sulfide Ore. U.S. Patent 2719082, 27 September 1955.
5. Van Weert, G.; Mah, K.; Piret, N.L. Hydrochloric acid leaching of nickeliferous pyrrhotite from the Sudbury District. *Bull. Can. Inst. Metall.* **1974**, *741*, 97–103.
6. Droppert, D.J.; Shang, Y. The leaching behaviour of nickeliferous pyrrhotite concentrate in hot nitric acid. *Hydrometallurgy* **1995**, *39*, 169–182. [CrossRef]
7. Thornhill, P.G. Autoclave Treatment of Pyrrhotite for Sulfur Recovery. *Can. Metall. Q.* **1969**, *8*, 219–225. [CrossRef]
8. Garg, S.; Papangelakis, V.G.; Mahadevan, R.; Edwards, E.; Krause, E. Bioleaching of Pyrrhotite Tailings for Ni Extraction—Initial Scoping Tests. In *Towards Clean Metallurgical Processing for Profit, Social and Environmental Stewardship*, Proceedings of the 51st Conference of Metallurgists COM12, Niagara Falls, ON, Canada, 30 September–3 October 2012; pp. 315–329; Shoonewille, R.H., Rioux, D., Kashani-Nejad, S., Kreuh, M., Muinonen, M.E.S., Eds.; Canadian Institute of Mining Metallurgy and Petroleum: Montreal, QC, Canada, 2012.

9. Beolchini, F.; Veglio, F. Kinetic modeling of pyrrhotite ore leaching by ferric iron and related statistical analysis. *Am. Chem. Soc.* **1999**, *38*, 3296–3299.
10. Janzen, M.P.; Nicholson, R.V.; Scharer, J.M. Pyrrhotite reaction kinetics: Reaction rates for oxidation by oxygen, ferric iron, and for nonoxidative dissolution. *Geochim. Cosmochim. Acta* **2000**, *64*, 1511–1522. [CrossRef]
11. Nicholson, V.R. Iron-sulfide oxidation mechanisms: Laboratory studies. In *Environmental Geochemistry of Sulfide Mine-Waste*; Jambor, J.L., Blowes, D.W., Eds.; Short Course Handbook on Environmental Geochemistry; Mineralogical Association of Canada: Quebec City, QC, Canada, 1994; Volume 22, pp. 163–183.
12. Subramanian, K.N.; Stratigakos, E.S.; Jennings, P.H. Hydrometallurgical processing of pyrrhotite. *Can. Metall. Q.* **1972**, *11*, 425–434. [CrossRef]
13. Steger, H.F.; Desjardins, L.E. Oxidation of sulfide minerals, 4. Pyrite, chalcopyrite and pyrrhotite. *Chem Geol.* **1978**, *23*, 225–237. [CrossRef]
14. Dutrizac, J.E. Elemental sulfur formation during the ferric sulfate leaching of chalcopyrite. *Can. Metall. Q.* **1989**, *28*, 337–344. [CrossRef]
15. McGuire, M.M.; Hamers, R.J. Extraction and Quantitative Analysis of Elemental Sulfur from Sulfide Mineral Surfaces by High-Performance Liquid Chromatography. *Environ. Sci. Technol.* **2000**, *34*, 4651–4655. [CrossRef]
16. Mendham, J.; Denney, R.C.; Barnes, J.D.; Thomas, M. *Vogel's Textbook of Quantitative Chemical Analysis*, 6th ed.; Prentice Hall: Upper Saddle River, NJ, USA, 2000.
17. Levenspiel, O. *Chemical Reaction Engineering*, 2nd ed.; John Wiley & Sons: Hoboken, NJ, USA, 1972; pp. 359–374.
18. Corrans, I.J.; Scholtz, M.T. A kinetic study of the leaching of pentlandite in acidic ferric sulfate solutions. *J. S. Afr. Inst. Min. Metall.* **1976**, *76*, 403–411.
19. Jena, P.K.; Barbosa-Filho, O.; Vasconcelos, I.C. Studies on the kinetics of slurry chlorination of a sphalerite concentrate by chlorine gas. *Hydrometallurgy* **1999**, *52*, 111–122. [CrossRef]
20. Gbor, P.K.; Jia, C.Q. Critical evaluation of coupling particle size distribution with the shrinking core model. *Chem. Eng. Sci.* **2004**, *59*, 1979–1987. [CrossRef]
21. Lngraham, T.F.; Parsons, H.W.; Cabri, L.J. Leaching of pyrrhotite in hydrochloric acid. *Can. Metall. Q.* **1972**, *11*, 407–411. [CrossRef]